Application of x-ray microtomography to environmental fluid flow problems

D. Wildenschild[*a,c], K.A. Culligan[b], and B.S.B. Christensen[c]
[a] Dept. of Geosciences, Oregon State University, Corvallis, OR 97331
[b] Dept. of Civil Engineering and Geol. Sciences, University of Notre Dame, Notre Dame, IN 46556
[c] Environment and Resources, Technical University of Denmark, DK-2800 Lyngby, Denmark

ABSTRACT

Many environmental processes are controlled by the micro-scale interaction of water and air with the solid phase (soils, sediments, rock) in pore spaces within the subsurface. The distribution in time and space of fluids in pores ultimately controls subsurface flow and contaminant transport relevant to groundwater resource management, contaminant remediation, and agriculture. Many of these physical processes operative at the pore-scale cannot be directly investigated using conventional hydrologic techniques, however recent developments in synchrotron-based micro-imaging have made it possible to observe and quantify pore-scale processes non-invasively. Micron-scale resolution makes it possible to track fluid flow within individual pores and therefore facilitates previously unattainable measurements. We report on experiments performed at the GSECARS** (Advanced Photon Source) microtomography facility and have measured properties such as porosity, fluid saturation and distribution within the pore space, as well as interfacial characteristics of the fluids involved (air, water, contaminant). Different image processing techniques were applied following mathematical reconstruction to produce accurate measurements of the physical flow properties. These new micron-scale measurements make it possible to test existing and new theory, as well as emerging numerical modeling schemes aimed at the pore scale.

Keywords: x-ray microtomography, multi-phase flow, micro-imaging, NAPL, capillary pressure-saturation relationship

1. INTRODUCTION

One of the most difficult and puzzling of groundwater flow problems is that of multi-phase flow; that is when two or more immiscible fluids are flowing through the same pore space. This happens above the groundwater table where air and water share the available pore space, and also when a contaminant (e.g. non-aqueous phase liquid, NAPL) phase is present either above or below the groundwater table. Many groundwater contamination problems result from a spill or release of NAPLs into the subsurface. Understanding the flow and transport of these multiple phases is of vital importance to practices such as remediation of contaminated aquifers, management and optimization of irrigation resources, and enhanced oil and gas recovery. Interfaces between the various phases, as illustrated in Figure 1, are crucial to this understanding.

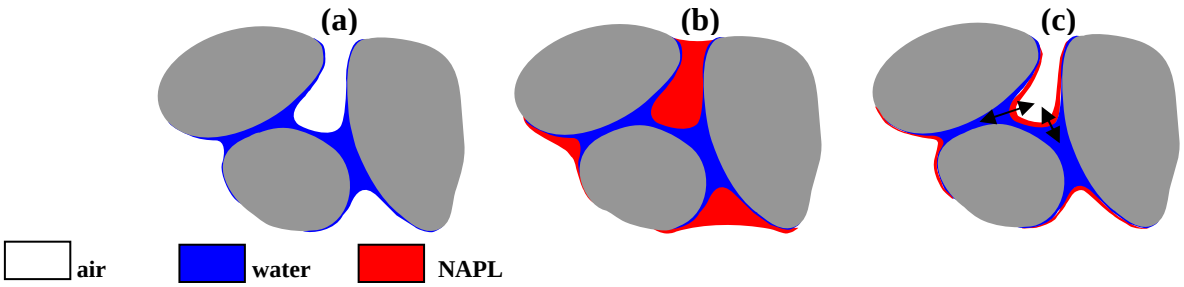

Figure 1. (a) air-water interfacial system, **(b)** NAPL-water interfacial system, **(c)** air-water-NAPL system with arrows indicating mass transfer across a NAPL-water interface

*wildend@geo.oregonstate.edu

**GeoSoil EnviroCARS, CARS: Consortium for Advanced Radiation Sources

For instance, fluid-fluid interfaces significantly impact the rate at which NAPL can be dissolved into the water phase, thus affecting potential cleanup scenarios, and how air and water is distributed in the pore space. The latter is of particular relevance to agricultural irrigation practices and nutrient uptake processes. In addition, interfaces have come to be seen as one of the key physical quantities in describing the physics of multi-phase flow.

A common problem in understanding these multi-phase flow processes is the lack of information about the porous medium and the processes governing flow and transport at the pore-scale in a porous material. In recent years, there has been an increased interest in simulating pore-scale topics using techniques such as the Lattice-Boltzmann method, network modeling, as well as other advanced computational fluid dynamics approaches, from researchers in engineering, soil science, water resources, and the petroleum industry. An argument can easily be made that a fundamental understanding of flow and transport mechanisms in porous media can be achieved only by studying pore-scale processes. These mechanisms operating at the micro-scale cannot be measured with traditional techniques, which generally require insertion of a sensor at or near the region of interest. Computed x-ray microtomography (CMT) overcomes this problem via the non-invasive observation of pore structure, as well as fluid phase and associated contaminant behavior. We have used CMT to accurately measure porosity, fluid saturation level and distribution[1,2,3], as well as interfacial characteristics such as the specific interfacial area between two phases sharing the pore space[2,3]. In this work we present results for two different research topics and porous media; (1) flow rate effects in a sandy soil sample, and (2) characterization of interfacial properties for quartz-glass bead packs. The research presented here are examples of the type of qualitative and quantitative information that can be obtained with the technique of relevance to environmental fluid flow problems.

1.1. Flow rate effects

Two important relationships need to be established prior to an investigation of a multi-phase flow problem: the functional dependence of pore or capillary pressure (P_c) on fluid saturation (S), and the relationship between fluid permeability and saturation. In this work, we will focus on the former relationship: An example is shown in Figure 2a. In the past, we have found that the manner in which water is drained from a porous material (soil, rock, or glass beads as a proxy) can play a major role in the resulting measurement of the interdependence of capillary pressure and saturation, the P_c-S relationship[4]. An example of this is illustrated in Figure 2b; clearly relatively large variations can be the result of using different drainage methodologies for this porous material. We have used CMT in this, and other research efforts, to try and understand why this phenomenon is observed for some, but not all porous materials that we have tested.

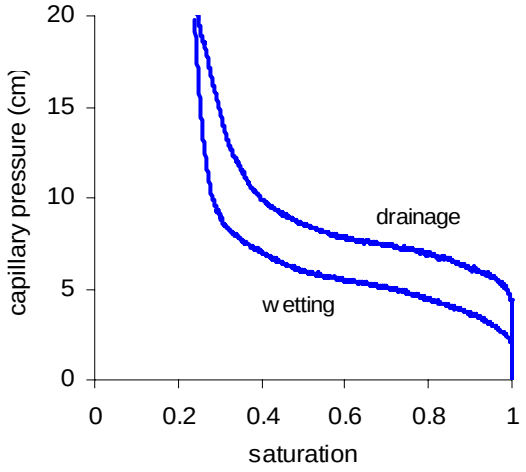

Figure 2a. Typical hysteretic relationship between capillary pressure and saturation for a sandy material.

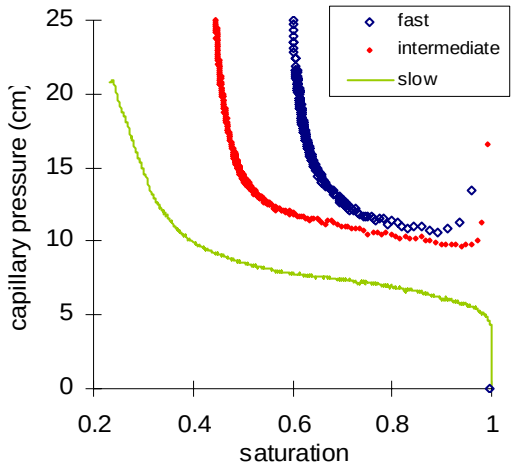

Figure 2b. Example of the effect of drainage flow rate (fast, intermediate, slow) on the resulting measured relationship between capillary pressure and saturation for a coarse sandy material.

1.2. Interfacial characterization

Over the years, many experimental techniques have been developed to measure the capillary pressure-saturation relationship, yet, its estimation often leaves the investigator confused because the functions are hysteretic, i.e., different curves are obtained for drainage and wetting conditions, see Figure 2a. Traditionally, the hysteresis present in capillary pressure-saturation curves has been attributed to two causes: contact angle hysteresis and pore geometry. However, according to Hassanizadeh and Gray[5] many researchers agree that hysteresis is related to the configuration and distribution of interfaces. Their theory states that the capillary pressure is a unique, non-hysteretic function of the curvature of the interfaces between the phases, and hysteresis in the P_c-S relationship is due to the choice of functional dependence, which excludes the air-water interfacial area. If capillary pressure is considered a function of two independent variables: saturation and interfacial area, hysteresis would be minimized. Thus, hysteresis might be interpreted as nothing but the projection of the capillary pressure-saturation-interfacial area surface onto the capillary pressure-saturation plane. While this hypothesis has been investigated using numerical techniques[6,7,8], physical experimental support has been lacking. Thus far, the opaque nature of porous media systems has precluded the possibility of observing microscale quantities such as fluid distribution and interfaces in-situ. However, with the availability of micro-imaging, it is now possible to provide further insight into this issue.

2. EXPERIMENTS

Very briefly, CMT is a technique for determining the internal structure of an object. It uses projection views (radiographs) from different angles to mathematically reconstruct the complete three-dimensional image of the object. The physical basis for the technique is the absorption or attenuation of the penetrating electromagnetic radiation by the object. The attenuation depends on the density and the atomic constituents of the material that is scanned and the transmitted radiation is compared to the incident radiation to reconstruct a map of attenuation coefficients versus position in the object.

The experiments presented here were conducted at the GeoSoilEnviro Consortium for Advanced Radiation Sources (GSECARS) bending magnet beamline, Sector 13, Advanced Photon Source (APS), Argonne National Laboratory. With the exception of the CCD camera and monochromator, the experimental setup used to obtain the three-dimensional images is the same as that described by Wildenschild et al.[1,9]. By adding a dopant (KI) to the fluid phase and scanning slightly above the peak absorption energy for iodide (33.17 keV), we achieved sufficient contrast between air/oil and water phases and could thereby resolve the distribution of the phases as a function of varying flow conditions. Using the GSECARS CMT facility we scanned cylindrical samples of sand-packs (6 mm inside diameter) during drainage, as well as glass-bead packs (7 mm inside diameter) during both drainage and wetting. Two different types of experiments were performed on the sand samples: (1) so-called one-step experiments where drainage was induced with one relatively high air-phase pressure and (2) multi-step experiments where a varying number of smaller pressure increments were applied, so that the water was drained slowly from the sample. Spatial and temporal changes in water saturation can then be compared for cases where different fluid flow rates apply. For the glass-bead samples we obtained data under quasi-static conditions both for air-water and oil-water systems. The basic setup is shown in Figures 3a and 3b; more details of the experimental procedure can be found in Wildenschild et al.[1,9].

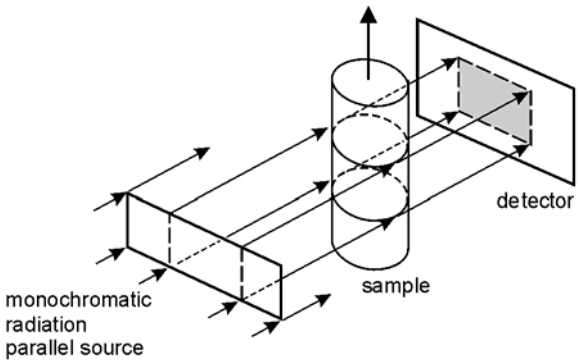

Figure 3a. Basic illustration of the microtomography beam-line setup at GSECARS showing the parallel beam and detector arrangement.

The microtomography stage setup at GSECARS is such that the samples can be translated and rotated under computer control in the beam. Since the detector consists of a two-dimensional array (CCD camera), a complete three-dimensional image is obtained in each scan/rotation, see Figures 3a and 3b. The raw data used for tomographic reconstruction are 12-bit images and a total of 360 such images were collected as the sample was rotated twice from 0 to 180 degrees in 0.5-degree steps. Reconstruction was achieved with a code written by Rivers[10] using IDL® programming and the Gridrec FFT (fast Fourier transform) reconstruction software developed at Brookhaven National Laboratory. This code incorporates dark current and white field normalization, filtering prior to back-projection, centering of the sinogram, ring artifact reduction, and zinger removal. The output from the reconstruction algorithm is a three-dimensional array of grey-scale intensities. The pixel values of the reconstructed images reflect absolute linear absorption coefficient in units of inverse pixel size. Dividing by the pixel size, say in mm/pixel yields the linear attenuation per mm. In all the grey-scale images presented here, white/light gray represents the water phase (high attenuation), black is the air phase, and the darker gray is the solid phase. Starting with the grey-scale data, we use a combination of various image processing techniques to arrive at images where the data is classified into its three main components; the non-wetting phase (air or oil), the wetting phase (water), and solid (sand or glass beads). When a true segmentation of all three phase is needed we use an image of the dry porous medium to subtract out the solid phase, and then a k-means cluster analysis routine is used to separate the remaining two phases. Prior to this, various filters and dilation and erosion processes are used. The image processing approach used is described in full detail in a previous publication[11]. Table 1 contains more details about the images obtained.

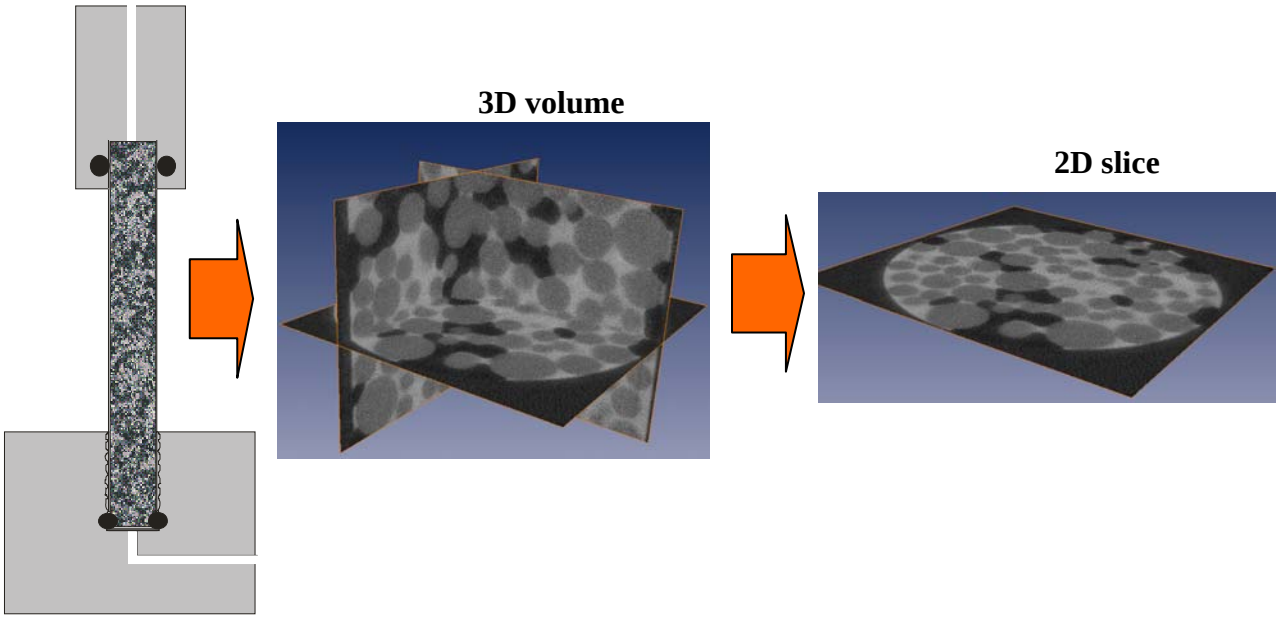

Figure 3b. The sample holder design and examples of the obtained 3D and 2D images.

Table 1. Imaging specifics

Exp. run	Energy (keV)	Number of view angles/step size (°)	Pixel size (μm/pixel)	exposure time (sec.)	Field of view width x height	Volume size (voxels)	Imaging objective
coarse sand	33.70	360/0.5 2 passes	17.5	9.3	11.50 x 4.10 (11.50 x 1.4)[§]	657*657*234	5x
glass beads	33.3	360/0.5 2 passes	17.0	0.65	11.05 x 5.10	650*650*300	5x

[§] Due to incident beam quality and resulting non-uniformity in the frames, only the middle 1.4 mm of the field of view was used in the quantitative analyses.

3. RESULTS AND DISCUSSION

3.1. Sand experiments - effect of drainage flow rate

The porous material used for investigating the flow rate phenomenon was a coarse sandy material, namely a crushed volcanic tuff, consisting mainly of quartz. The sand also contained small amounts of various other minerals such as feldspar, albite, and volcanic glasses. The material was packed in the 6 mm i.d. sample holder (Figure 3b) to a porosity of 44%. As mentioned earlier, we had found inconsistencies in the P_c-S relationship with drainage rate in past experiments using this material, see Figure 2b. The experiments were performed analogously to those described in detail in Wildenschild et al.[1]. Basically, two different kinds of drainage scenarios were used; (1) fast drainage using a high flow rate, facilitated by one large imposed air phase pressure step ("fast" in Figure 2b), and (2) slow drainage using a sequence of smaller pressure steps ("slow" in Figure 2b), eventually arriving at the same final capillary pressure.

The outcome of using these two different drainage processes are illustrated in the following: Figure 4 shows a vertical cross-section through the sample for slow drainage and fast drainage. Figure 5 illustrates similar conditions for a horizontal cross-section. Clearly, there is a difference in the amount of water drained from the sample under the two boundary conditions, and also in the distribution of the residual water in the sample. Under fast drainage conditions, a larger amount of water is being retained in the sample due to entrapment and loss of connection with the bulk water phase. When the sample is drained in numerous, smaller steps, water is allowed to redistribute during the process, and water phase continuity is preserved[1]. This results in a generally lower residual water saturation, which is illustrated quantitatively in Figure 6. Note that Figure 6 shows data for only the center 1.4 mm of the sample, whereas the images in Figure 4 represent the entire 4.1 mm imaged height of the sample. Due to problems with the beam-line monochromator at the time, we were only able to obtain a relatively uniform white field (image with no sample) for approximately 80 pixels in the vertical (1.4 mm at a pixel size of 17.5 micron) in the middle of our imaged section. Therefore, our quantitative analysis is restricted to this section of the sample.

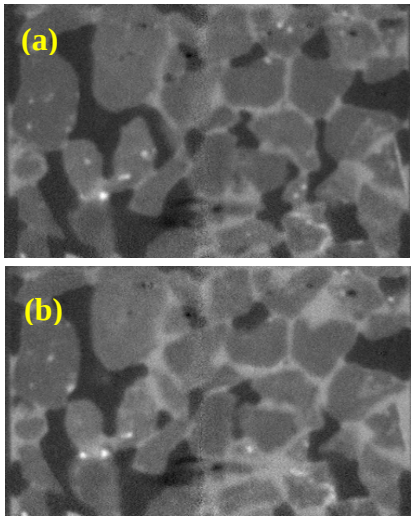

Figure 4. Vertical cross-sections for **(a)** slow drainage and **(b)** fast drainage (the higher density minerals appear as bright areas in the images).

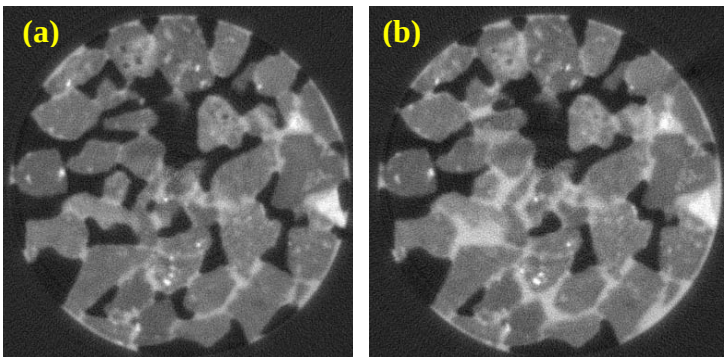

Figure 5. Horizontal cross-sections for **(a)** slow drainage and **(b)** fast drainage.

Three saturation profiles are illustrated in Figure 6. The saturated profile prior to starting the drainage process (blue circles), the profile after slow drainage (green triangles), and the profile after fast drainage (red crosses). Clearly, a large difference in final saturation is the result of the different flow rates. The average residual saturation for fast drainage is 0.30 and for slow drainage 0.18, a 67% difference when considering the slow drainage the method producing the most correct results.

Conceivably, draining the sample slowly will more closely simulate natural flow conditions, which are generally driven by gravity and capillarity only. Which leads us to conclude, that caution should be used when extrapolating P_c-S measurements obtained under fast conditions to naturally occurring processes that in general approach conditions that are closer to static. The one-step fast drainage technique was used quite widely for a number of years, but most researchers have now switched to the practice of using the slower multi-step approach instead[12]. In addition to these findings regarding measurement techniques, the results obtained here imply that there is some fundamental concept that we are unable to explain using traditional descriptions such as the Darcy and Richard's equations generally used for unsaturated or multi-phase flow. The fact that there appears to be dynamic processes involved, that we currently do not account for, has also been addressed by others recently[13,14,15].

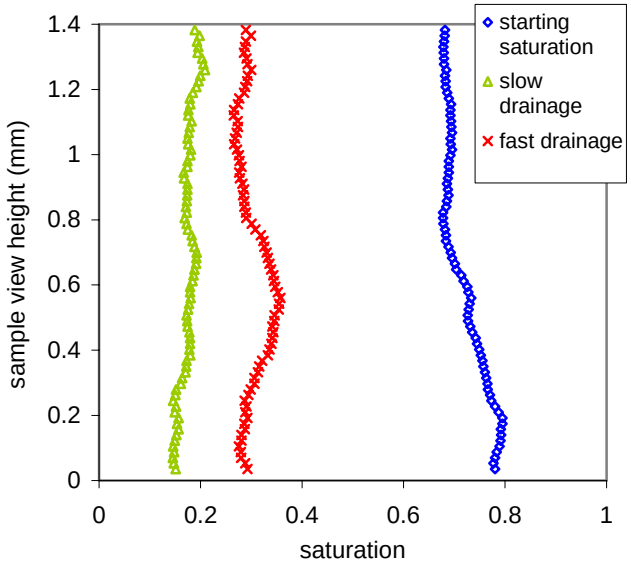

Figure 6. Vertical saturation profiles for the 1.4 mm imaged and processed section of the sample.

Obviously, the fact that our samples are three-dimensional needs to be taken into account when analyzing the data. The dynamic behavior that we are observing is to some degree influenced by the fact that pores can extend in three dimensions, and as such should not be interpreted in two dimensions, even though interpretation often is simplified by only considering two dimensions. Figures 4 and 5 compared cross-sections for either fast or slow drainage, yet in some cases, studying the full 3D image can provide new information about tortuosity and interconnectedness of the flow paths. We have included Figure 7 to illustrate the quality of the images obtained with CMT. In this figure, the full 3D effect of using the different flow rates is easily observed. And if loaded into a rendering program such as Amira©, it is possible to examine the images in even more detail, for instance with respect to the distribution and connectivity of the water phase (white areas) in the sample under the two different flow conditions.

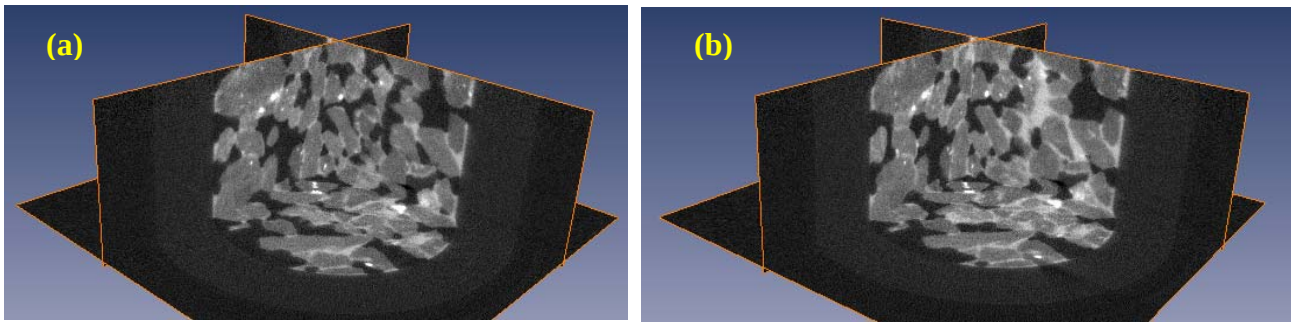

Figure 7. Three-dimensional rendering of the sample after **(a)** slow and **(b)** fast drainage

3.2. Glass-bead experiments – interfacial characteristics

The second part of this publication is concerned with the characterization of interfacial properties such as the fluid-fluid interfacial area. The interfacial area provides a measure of the area available to mass transfer, and therefore can be of great importance when dealing with clean-up methodologies such as vapor extraction, where the contaminants have to transfer across the interface to be effectively removed. We have used a well-defined distribution of glass beads as a proxy for a natural soil in this study, mainly to simplify the image processing part of the research. A 6 or 7 mm i.d. column (Figure 3b) was packed with soda lime glass beads to a porosity of 34%. Images were taken of a 5 or 6 mm

vertical section of a longer column for the air-water and oil-water systems, respectively. Both drainage and wetting experiments were performed to provide data for both types of processes. The main goal was to try and produce images of sufficient quality to extract reliable information about the interfacial area as a function of saturation and capillary pressure for both air-water and oil-water systems. We have examined both air-water and oil-water systems, because they both represent important subsurface flow and transport scenarios; relevant to irrigated agriculture, nutrient uptake etc. for the air-water system, and for the oil-water system of high relevance to remediation of for instance a NAPL spill in the subsurface.

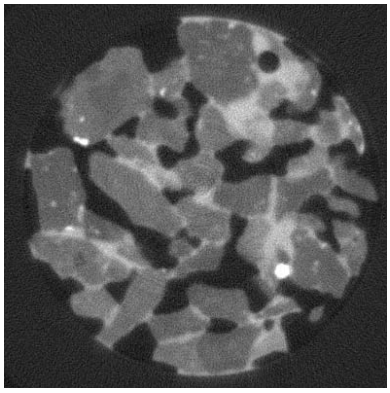

Figure 8a. The raw (greyscale) image.

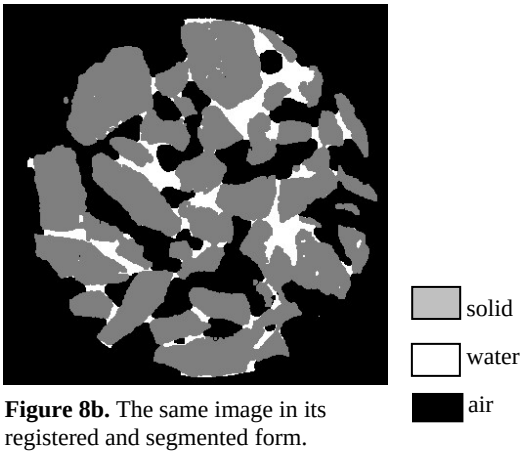

Figure 8b. The same image in its registered and segmented form.

Continuous drainage and wetting cycles were carried out to establish sufficient data to investigate the relationship between capillary pressure, saturation, and wetting-nonwetting interfacial area, the P_c-S-A_{wn} relationship. The wetting phase consists of water in both types of experiments, whereas, the nonwetting phase is either air or oil. The water was either drained out or pumped back into the sample using a precision syringe pump, and the pump stopped intermittently to scan the sample at various saturations. The experiments are described in detail in Culligan et al.[2] for the air-water system, and in Culligan et al.[3] for the oil-water system. All images were processed according to Wildenschild et al.[11] the final result being a complete segmentation of the three phases present in the sample; air/oil, water, and glass beads. An example of the images before and after segmentation is shown in Figure 8a and 8b representing the grey-scale and segmented images, respectively.

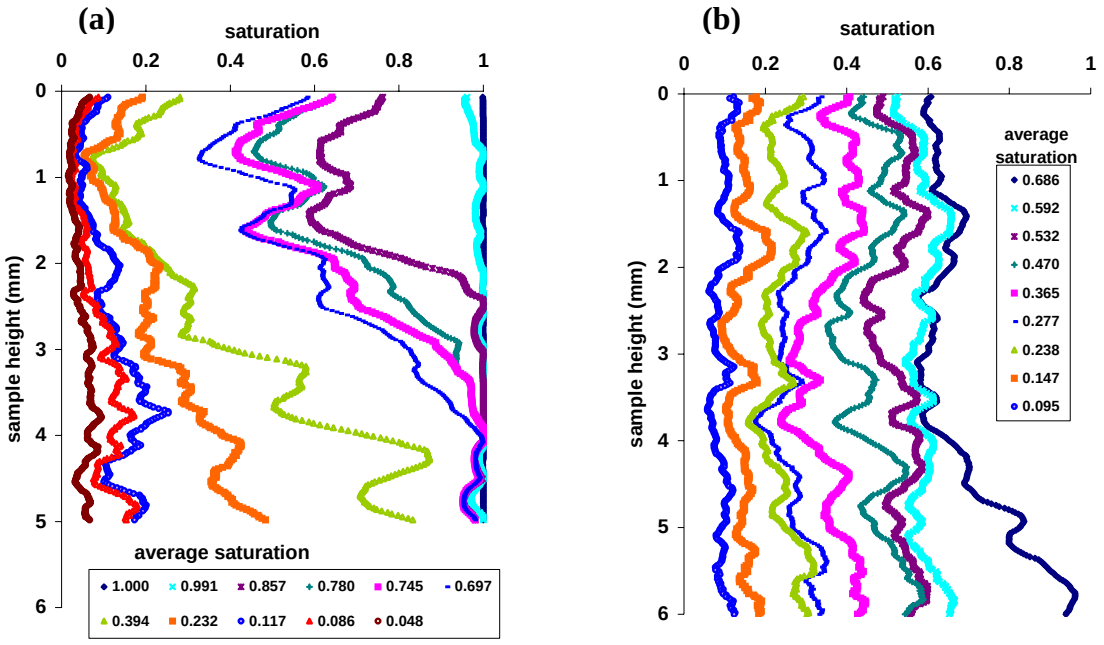

Figure 9. Vertical profiles for **(a)** air-water system, and **(b)** oil-water system.

After segmentation, the saturations of the various phases were calculated and vertical profiles established, see Figure 9. Figure 9a illustrates saturation as a function of sample height for the 5 mm tall imaged section of the air-water system, while Figure 9b shows the same data for the 6 mm tall imaged section of the oil-water system. Some interesting information can be extracted from these figures; as the sample drains (air or oil replacing water), very different drainage profiles are obtained. The air-water system starts from close to full saturation (S=1.0) and initially drains mostly from the top of the sample, and in a very non-uniform manner. The oil-water system starts from a relatively low initial saturation (S=0.69), and drains quite uniformly over the height of the sample.

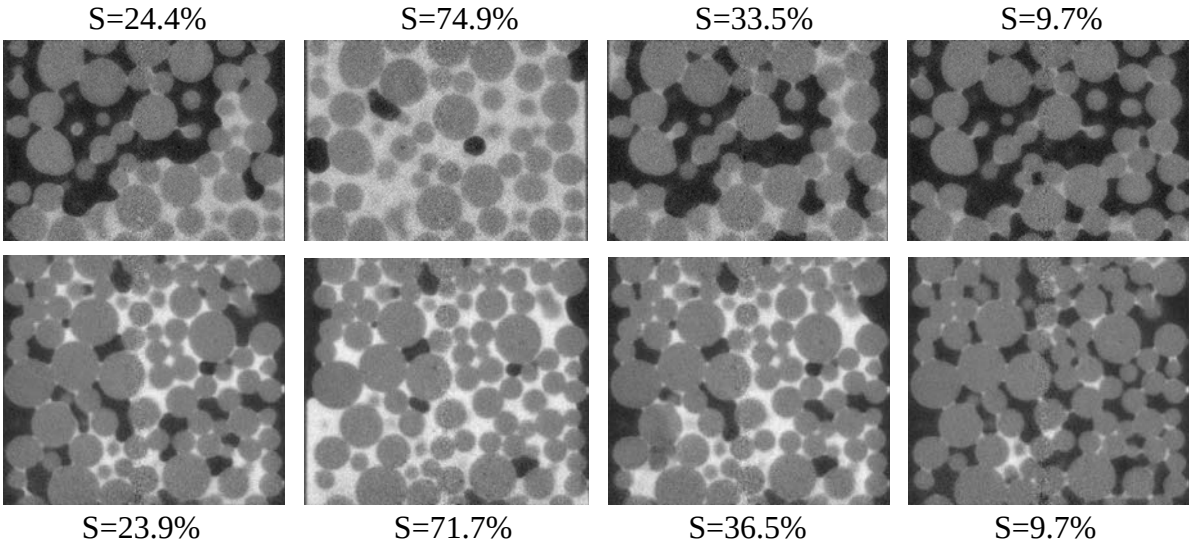

Figure 10. Air-water **(top row)** and oil-water **(bottom row)** systems at similar saturations and for glass bead packs with the same distribution of bead sizes.

This corresponds to the behavior we observed during the experiments: A large amount of trapped oil was left behind in disconnected pore space, and thus prevented the piston type drainage seen for the air-water system. This is also evident from the images shown in Figure 10, which is a collection of images for the two systems taken at similar saturations to allow for comparison. The air-water images in the top row for the intermediate saturations (24.4 and 33.5 %) show a very non-uniform distribution of water with very high saturation at the bottom of the sample, and very little water towards the top. This is a typical piston type flow situation where water enters from the bottom and drains from the top.

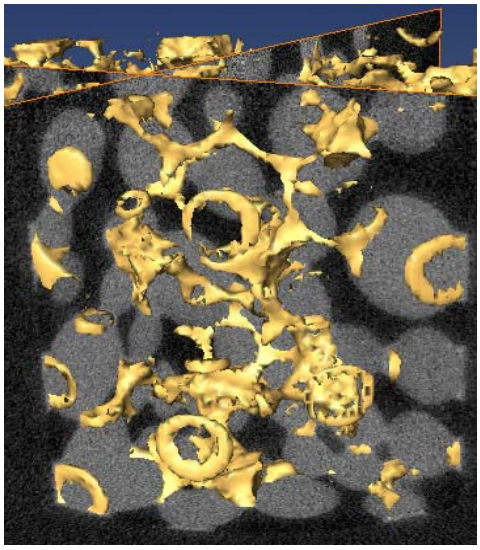

In comparison, the oil-water images at similar saturations (23.9 and 36.5%) show a much more even distribution of water.

As illustrated in Figure 11, very detailed three-dimensional information about one of the individual phases can be obtained for such a controlled and well-defined system. Figure 11 illustrates the presence of pendular rings of water between individual glass beads in a sample at residual water saturation. This configuration severely limits flow and the interfacial area will control contaminant mass transfer at this point. Quantifying the amount of interfacial area present in the sample under varying saturations was one of the main goals of this research using the glass bead packs. In the past, interfacial area measurements have been based on indirect measurements using interfacial tracers[16,17], but are uncertain because the portion of the fluid-fluid interface that is accessed by the tracer and included in the resulting measure is unclear.

Figure 11. Distribution and continuity of water phase at residual saturation. The majority of the fluid is contained in dead-end pore space and pendular rings between glass beads.

Also, the measurement provides information about how much interfacial area is present, but does not shed any light on the arrangement of the interfacial surfaces. Held and Celia[7] specifically call for measurement techniques capable of resolving non-traditional porous media variables such as interfacial areas and common lines (the contact points between the three phases). Yet, so far, experimentally measuring the interfacial area at the pore scale has proven to be a difficult task[7,6]. However, with the use of CMT we have been able to measure the wetting-nonwetting interfacial area for the glass beads samples with varying saturation. An example is shown in Figure 12 for both the air-water[2] and the oil-water[3] system.

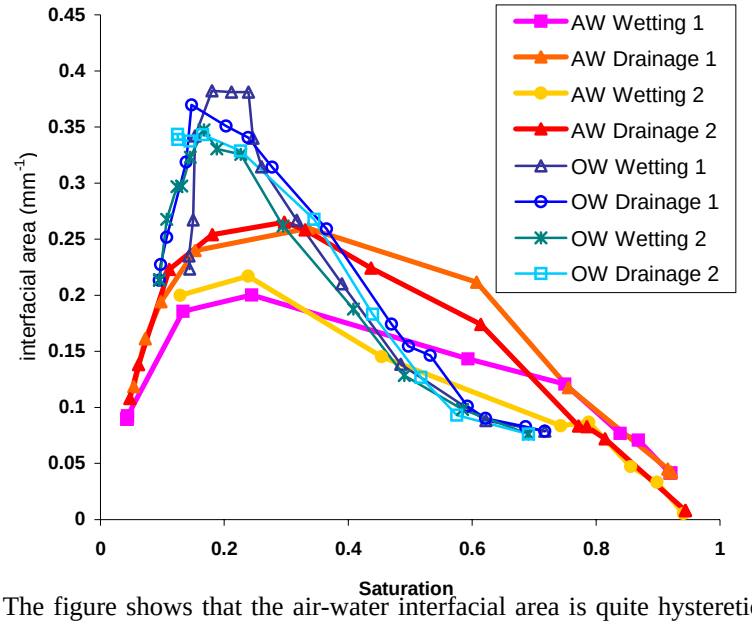

Figure 12. Wetting-nonwetting interfacial area measurements for air-water and oil-water systems in a glass bead-pack.

The figure shows that the air-water interfacial area is quite hysteretic; the wetting curves result in consistently lower interfacial area than the drainage curves. This is not the case for the oil-water system. Another interesting observation is the fact that a higher maximum interfacial area is obtained for the oil-water system at around 20-25% saturation. This is consistent with results illustrated in Figure 10; the oil-water system contains a more spatially distributed and fragmented water phase at 23.9% saturation, which results in a higher interfacial area between the water and oil phases. The results for the air-water system very closely match numerical simulations performed by Reeves and Celia[6] for drainage and wetting in a glass bead pack. Their system did not contain water films and currently, it is unlikely that our method is capable of detecting these either. However, with improvements in image resolution we hope to be able to also image fluid films in the future. Nevertheless, the fact that the air-water and oil-water systems behave so differently provides important information about how the differences in viscosity, wettability and relative permeability might influence the flow and transport behavior in the two systems.

The use of CMT facilitates high-quality pore scale data in a non-invasive manner, and is therefore going to be a valuable tool for evaluating theories and numerical models for multi-phase flow and transport in porous media. In terms of understanding multi-phase flow and improving current contaminant clean-up methodologies, it is encouraging that such detailed information can be obtained. Currently, there are no means for testing the validity of new theoretical and numerical approaches because there are very limited measurements available of pore scale properties such as fluid distribution and interfacial area. As the image resolution improves, future issues that can likely be addressed with CMT include biofilm behavior, as well as virus transport phenomena in subsurface porous media.

ACKNOWLEDGMENTS

The Danish Technical Research Council is gratefully acknowledged for financial support. Part of this research was carried out while one of the authors (Wildenschild) was employed at Lawrence Livermore National Laboratory and

thus part of this work was performed under the auspices of the U.S. Dept. of Energy by Lawrence Livermore National Laboratory under contract No. W-7405-ENG-48 and supported by the Environmental Management Science Program. Use of the Advanced Photon Source was supported by the DOE Basic Energy Sciences, Office of Science, under Contract No. W-31-109-ENG-38.

REFERENCES

1. Wildenschild, D., J.W. Hopmans, A.J.R. Kent, M.L. Rivers, 2004a. A Quantitative Study of Flow-Rate Dependent Processes Using X-ray Microtomography. Accepted by *Vadose Zone Journal*.
2. Culligan, K.A., D. Wildenschild, B.S.B. Christensen, W.G. Gray, A.F.B. Tompson, 2004a. Interfacial Area Measurements for Unsaturated Flow Through a Porous Medium. Accepted by *Water Resources Research*.
3. Culligan, K.A., D. Wildenschild, W.G. Gray, B.S.B. Christensen, M.L. Rivers, 2004b. Microscale and Macroscale Characteristics of Multiphase Flow in Porous Media: a Comparison of Air-Water and Oil-Water Experiments. Submitted to *Advances in Water Resources.*
4. Wildenschild, D., J.W. Hopmans, and J. Simunek, 2001. Flow rate dependence of soil hydraulic characteristics. *Soil Sci. Soc. Am. J.*, 65(1), 35-48.
5. Hassanizadeh, S.M. and W.G. Gray, 1993. Thermodynamic basis of capillary pressure in porous media. *Water Resources Research*, 29, 3389-3405.
6. Reeves, P.C., Celia, M.A., 1996. A functional relationship between capillary pressure, saturation, and interfacial area as revealed by a pore-scale network model. *Water Resources. Research*, 32 (8), 2345-235.
7. Held, R.J., Celia, M.A., 2001. Modeling support of functional relationships between capillary pressure, saturation, interfacial areas and common lines. Advances *in Water Resources* 24 (3-4), 325-343.
8. Dalla, E., M. Hilpert, and C.T. Miller, Computation of the interfacial area for two-fluid porous medium systems, *Journal of Contaminant Hydrology*, *56*, 25-48, 2002.
9. Wildenschild, D., J.W. Hopmans, C.M.P. Vaz, M.L. Rivers, and D. Rikard, Using X-Ray Computed Tomography in Hydrology: Systems, Resolutions, and Limitations, *Journal of Hydrology*, *267*(3-4), 285-297, 2002.
10. Rivers, M.L. 1998. Tutorial Introduction to X-ray Computed Microtomography Data Processing, http://www-fp.mcs.anl.gov/xray-cmt/rivers/tutorial.html
11. Wildenschild, D., K.A. Culligan, B.S.B. Christensen, M.L. Rivers, B.J. Joshi, 2004b. Image processing of grey-scale x-ray tomographic data using cluster analysis-based segmentation: A hydrologic application. Submitted to *Computers & Geosciences.*
12. Eching, S.O., J.W. Hopmans, and O. Wendroth, 1994. Unsaturated hydraulic conductivity from transient multistep outflow and soil water pressure data. *Soil Sci. Soc. Am. J.*, 58, 687-695.
13. Hassanizadeh, S.M., M.A. Celia, and H.K. Dahle, 2002. Dynamic Effect in the Capillary Pressure–Saturation Relationship and its Impacts on Unsaturated Flow, *Vadose Zone Journal* 1:38-57.
14. Mortensen, A.P., R.J. Glass, K.H. Hollenbeck and K.H. Jensen (2001). Visualization of microscale displacement processes in retention and outflow experiments: nonuniqueness of unsaturated flow properties, *Water Resources Research*, 37(6), 1627-1640.
15. Hollenbeck, K.J. and K.H. Jensen (1998). Experimental evidence of randomness and non-uniqueness in unsaturated outflow experiments designed for hydraulic parameter estimation, *Water Resources Research*, 34(4), 595-602.
16. Kim, H., P.S.C. Rao, and M.D. Annable, Determination of effective air-water interfacial area in partially saturated porous media using surfactant adsorption, *Water Resources Research*, *33*(12), 2705-2711, 1997.
17. Costanza-Robinson, M.S., and M.L. Brusseau, Air-water interfacial areas in unsaturated soils: Evaluation of interfacial domains, *Water Resources Research*, *38*(10), 1195, doi: 10.1029/2001WR000738, 2002.